JOURNAL OF MAGNETIC RESONANCE **135,** 133–143 (1998)
ARTICLE NO. MN981563

Signal Dynamics in Magnetic Resonance Imaging of the Lung with Hyperpolarized Noble Gases

Harald E. Möller,[1] X. Josette Chen, Mark S. Chawla, Bastiaan Driehuys,* Laurence W. Hedlund, and G. Allan Johnson

*Center for In Vivo Microscopy, Duke University Medical Center, Durham, North Carolina 27710; and *Magnetic Imaging Technologies Inc., Durham, North Carolina 27713*

Received January 13, 1998; revised July 6, 1998

The nonequilibrium bulk magnetic moment of hyperpolarized (HP) noble gases generated by optical pumping has unique characteristics. Based on the Bloch equations, a model was developed describing the signal dynamics of HP gases used in magnetic resonance imaging (MRI) of the lung with special consideration to the breathing cycle. Experimental verification included extensive investigations with HP ^{3}He and ^{129}Xe during both inspiration and held breath in live guinea pigs. Radial acquisition was used to investigate the view variations with a temporal resolution of 5 ms. Agreement between theoretical predictions and *in vivo* results was excellent. Additionally, information about effects from noble gas diffusion and spin–lattice relaxation was obtained. *In vivo* results for T_1 were 28.8 ± 1.8 s for ^{3}He and 31.3 ± 1.8 s for ^{129}Xe. Comparison with *in vitro* data indicated that relaxation in the pulmonary gas space is dominated by dipolar coupling with molecular oxygen. The results provide a quantitative basis for optimizing pulse sequence design in HP gas MRI of the lung.

Key Words: **bulk magnetic moment dynamics; ^{3}He NMR; hyperpolarized noble gases; lung MRI; ^{129}Xe NMR.**

INTRODUCTION

An elegant approach toward overcoming the inherently low sensitivity of NMR is to produce a large nonequilibrium polarization in noble gases by spin exchange with optically pumped rubidium vapor (*1*). Because spin–lattice relaxation limits the accumulation of angular momentum by the nucleus, the two spin-$\frac{1}{2}$ noble gas isotopes ^{3}He and ^{129}Xe stand out due to their very long T_1. Procedures to obtain liter quantities of highly polarized gas have already been described (*2, 3*). Alternatively, optically pumping metastable states and allowing metastability exchange collisions may be used as an efficient technique for polarizing ^{3}He (*4*). Applications of hyperpolarized (HP) noble gases span a wide variety of disciplines. In particular, the recent success in enhancing magnetic resonace imaging (MRI) of lung gas spaces (*5–16*) has demonstrated the potential for a promising research and clinical tool in biomedical imaging.

Compared with conventional ^{1}H MRI, lung imaging with HP gases has several unique properties. (i) It allows direct imaging of the air spaces, which was previously not possible with proton techniques. (ii) The strength of the bulk magnetic moment produced by optical pumping does not depend upon the external magnetic field, B_0. (iii) Due to the nonequilibrium state of the magnetic moment, there is no recovery of signal between successive excitations (views). (iv) The choice of the repetition time has no impact on the contrast. (v) Significant consequences may arise from diffusion, as typical diffusion coefficients in gases are five orders of magnitude greater than in water.

Recently, we demonstrated that by varying flip angle and sequence timing a variety of features can be imaged, ranging from images of the fully filled lungs to visualization of pulmonary airways down to about 6th generation (*16*). In the present study, we report detailed theoretical analysis of experimental signal curves measured during inspiration and held breath. Radial acquisition (RA) was used because it facilitates measurement of the magnetic moment during image acquisition at temporal sampling in the millisecond range.

THEORY

Three compartments exchanging HP gas during the respiratory cycle are considered in our model, as shown in Fig. 1a. HP gas is supplied from an external reservoir, R, with a macroscopic magnetic moment at time zero, $M_{z,R}(0)$, of (*6*),

$$M_{z,R}(0) = \tfrac{1}{2}\, N_R(0)\, P\gamma\hbar, \qquad [1]$$

where N_R is the number of resonant nuclei (^{3}He or ^{129}Xe) in the reservoir, P is the polarization at the beginning of the experiment, γ is the gyromagnetic ratio, and $\hbar$ is Planck's constant. Neglecting the small thermal polarization contribution (*17*), $M_{z,R}$ decays with a characteristic time $T_{1,R}$ according to

$$M_{z,R}(t) = M_{z,R}(0)\exp(-t/T_{1,R}). \qquad [2]$$

The imaging strategy we are considering is the acquisition of a free induction decay (FID) with RA (*18*). We denote $\mathbf{M}_p(n_j^-)$ and $\mathbf{M}_p(n_j^+)$ the magnetic moment in the pulmonary gas space, p, just before and immediately after the nth radiofrequency

[1] To whom correspondence should be addressed. E-mail:hem@orion.mc.duke.edu.

1090-7807/98 $25.00

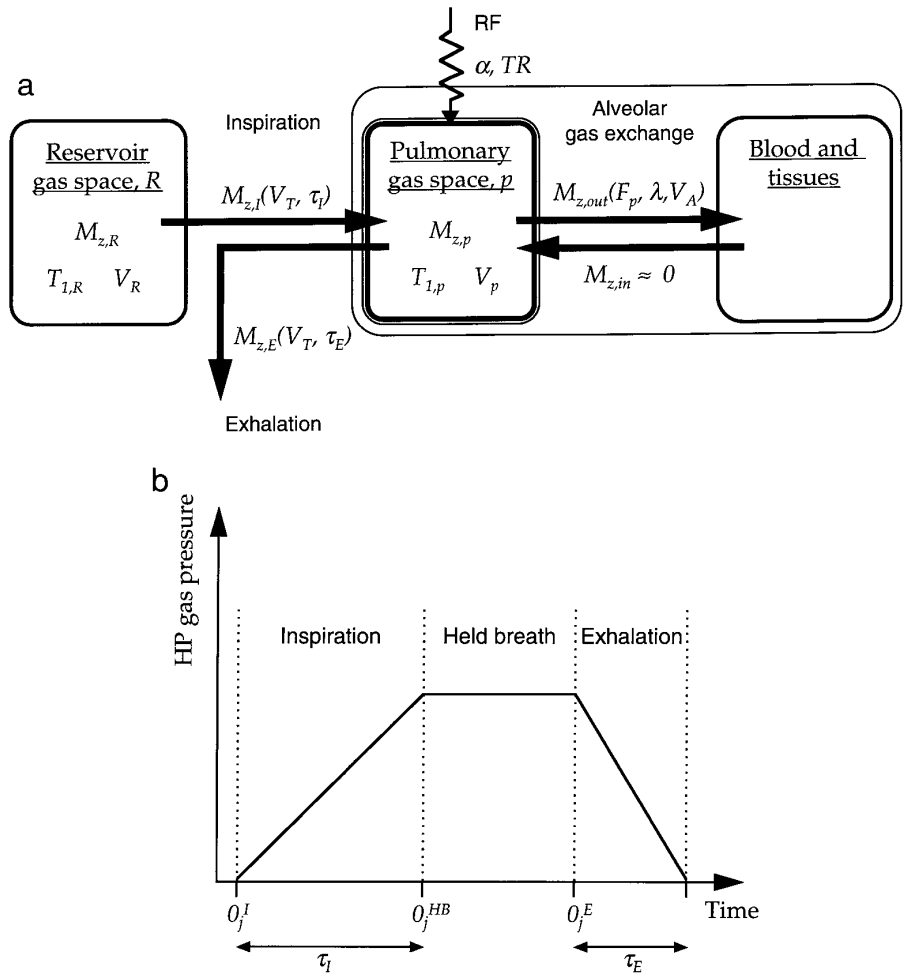

FIG. 1. (a) Flow diagram of the model used to calculate MRI signal dynamics. We consider a situation where HP gas is contained in an external volume, V_R, and administered to an animal lung in increments of the tidal volume, V_T. The magnetic moment in this reservoir, $M_{z,R}$, decays with a characteristic time $T_{1,R}$. Each inspiration (duration τ_I) delivers a magnetic moment $M_{z,I}$ to the pulmonary gas space, V_p. In the lung, the pulmonary magnetic moment, $M_{z,p}$, decays via spin–lattice relaxation (described by $T_{1,p}$), alveolar gas exchange (depending on the pulmonary blood flow, F_p, the partition coefficient, λ, and the alveolar volume, V_A), and RF pulsing (characterized by the flip angle α and the repetition time TR). Effects from RF pulsing on the magnetic moment in blood and tissues are not discussed here although we note that partial excitation depending on the bandwidth of the pulse and the resonance offset from the gas phase signal may occur. Finally, a magnetic moment $M_{z,E}$ is lost during exhalation (duration τ_E). (b) Timing diagram of HP gas administration (described by the partial pressure P) to the animal lung during the jth noble gas breath. The time at the beginning of inspiration, held breath, and exhalation is indicated by 0_j^I, 0_j^{HB}, and 0_j^E, respectively.

(RF) pulse (flip angle α) of the jth breath. Without loss of generality, we assume that the pulse is applied on resonance along the rotating frame x axis and that the total transverse magnetic moment from the previous excitation has decayed to zero due to dephasing gradients. Thus,

$$\mathbf{M}_p(n_j^+) = \begin{pmatrix} 0 \\ M_{z,p}(n_j^-)\sin\alpha \\ M_{z,p}(n_j^-)\cos\alpha \end{pmatrix}. \quad [3]$$

During the period TR between pulses, $M_{z,p}$ decays with a characteristic time $T_{1,p}$ due to spin–lattice relaxation. In addition, a fraction of the alveolar gas is removed by means of the pulmonary blood flow F_p. Assuming that tissue relaxation occurs more quickly than recirculation, we may characterize this flux by first order kinetics with a rate constant $k_{out} = F_p\lambda/V_A$, where λ is an appropriate partition coefficient between blood and alveolar gas space and V_A is the total alveolar volume (*19*). Finally, polarized spins enter the lung from the reservoir during inspiration. A simplified timing diagram is shown in Fig. 1b. For constant influx with a tidal volume V_T, an initial volume $V_R(0)$ of the gas reservoir, and an inspiration period τ_I, the magnetic moment delivered by ventilation during each interval TR is

$$M_{z,I}(t) = M_{z,R}(0)\,\frac{V_T}{V_R(0)}\,\frac{TR}{\tau_I}\exp(-t/T_{1,R})$$

$$= M_{z,I}(0)\exp(-t/T_{1,R}). \quad [4]$$

The initial portion inhaled at the beginning of the jth breath is thus

$$M_{z,I}(0_j) = M_{z,I}(0)\exp[-(j-1)\cdot\Delta\tau_I/T_{1,R}], \quad [5]$$

where $\Delta\tau_I$ is the time between subsequent noble gas breaths. Consequently, we obtain for the total pulmonary magnetic moment before the $(n+1)$st RF pulse

$$M_{z,p}(n+1_j^-) = M_{z,p}(n_j^+)\exp(-TR/T_{1,p})\exp(-k_{out}\cdot TR) + M_{z,I}(0_j)\exp(-n\cdot TR/T_{1,R}). \quad [6]$$

We may now use the nomenclature described above and Eqs. [3] and [6] to calculate time courses of the signal during the jth ventilatory cycle. If a fraction $M_{z,p}(0_j^I)$ is left in the lung from previous breaths, the total magnetic moment seen by the first RF pulse during inspiration is $M_{z,p}(0_j^I) + M_{z,I}(0_j)$, and we obtain

$$M_{z,p}(1_j^+) = [M_{z,p}(0_j^I) + M_{z,I}(0_j)]\cos\alpha, \quad [7]$$

$$M_{z,p}(2_j^-) = [M_{z,p}(0_j^I) + M_{z,I}(0_j)]E_{1,p}\cos\alpha + M_{z,I}(0_j)E_{1,R}. \quad [8]$$

In Eq. [8], we use an apparent spin–lattice relaxation rate $1/T'_{1,p} = k_{out} + (1/T_{1,p})$ for the combined effects of polarization loss (i.e., blood uptake and relaxation) and abbreviations $E_{1,p} = \exp(-TR/T'_{1,p})$ and $E_{1,R} = \exp(-TR/T_{1,R})$. After the second pulse, we find

$$M_{z,p}(2_j^+) = [M_{z,p}(0_j^I) + M_{z,I}(0_j)]E_{1,p}\cos^2\alpha + M_{z,I}(0_j)E_{1,R}\cos\alpha, \quad [9]$$

$$M_{z,p}(3_j^-) = [M_{z,p}(0_j^I) + M_{z,I}(0_j)]E_{1,p}^2\cos^2\alpha + M_{z,I}(0_j)E_{1,R}E_{1,p}\cos\alpha + M_{z,I}(0_j)E_{1,R}^2. \quad [10]$$

Continuing in identical fashion, the following general representation is obtained with some algebra:

$$M_{z,p}(n_j^-) = M_{z,p}(0_j^I)E_{1,p}^{n-1}\cos^{n-1}\alpha + M_{z,I}(0_j)E_{1,R}^{n-1}\frac{1-(E_{1,p}/E_{1,R})^n\cos^n\alpha}{1-(E_{1,p}/E_{1,R})\cos\alpha}. \quad [11]$$

With Eq. [3], the signal amplitude of the nth view measured during constant inspiration (jth breath) of HP gas is therefore

$$S_I(n_j) \propto M_{z,p}(0_j^I)E_{1,p}^{n-1}\cos^{n-1}\alpha\sin\alpha + M_{z,I}(0_j)E_{1,R}^{n-1}\frac{1-(E_{1,p}/E_{1,R})^n\cos^n\alpha}{1-(E_{1,p}/E_{1,R})\cos\alpha}\sin\alpha. \quad [12]$$

If RF pulsing is restricted to periods of held breath, a similar calculation yields

$$S_{HB}(n_j) \propto M_{z,p}(0_j^{HB})E_{1,p}^{n-1}\cos^{n-1}\alpha\sin\alpha, \quad [13]$$

which agrees with earlier predictions (*15–17*). In Eq. [13], $M_{z,p}(0_j^{HB})$ comprises contributions from previous breaths and the magnetic moment delivered to the lungs with the jth inspiration according to

$$M_{z,p}(0_j^{HB}) = M_{z,p}(0_j^I)\exp(-\tau_I/T'_{1,p}) + M_{z,R}(0)\frac{V_T}{V_R(0)}\times\exp[-(j-1)\cdot\Delta\tau_I/T_{1,R}]. \quad [14]$$

Finally, scanning during expiration can be treated in analogy to inspiration, replacing $M_{z,I}(t)$ with $-M_{z,E}(t)$, the fraction of magnetic moment lost during each TR interval by exhaling:

$$M_{z,E}(t) = M_{z,E}(0_j^E)\frac{V_T}{V_R(0)}\frac{TR}{\tau_E}\exp(-t/T'_{1,p}) = M_{z,E}(0_j)\exp(-t/T'_{1,p}). \quad [15]$$

$M_{z,p}(0_j^E) = M_{z,p}(0_j^{HB})\exp(-\tau_{HB}/T'_{1,p})$ is the magnetic moment left in the lung immediately before the jth expiration, V_p is the volume of the pulmonary gas space, and τ_{HB} and τ_E are the durations of held breath and expiration, respectively. Calculation of the signal amplitude yields

$$S_E(n_j) \propto M_{z,p}(0_j^E)E_{1,p}^{n-1}\cos^{n-1}\alpha\sin\alpha - M_{z,E}(0_j)E_{1,p}^{n-1}\frac{1-\cos^n\alpha}{1-\cos\alpha}\sin\alpha. \quad [16]$$

The first term in Eq. [16] is formally identical to the held breath result, Eq. [13], while the second term describes the additional loss of polarization due to exhalation of HP gas before contributing to the signal. As scanning during expiration obviously wastes hyperpolarization, it was not further considered in this study. The prediction of an accelerated decay compared with imaging during held breath agrees perfectly, however, with previous experimental observations (*15*).

EXPERIMENTAL

Laser-Polarization and HP Gas Delivery

Noble gases were hyperpolarized by spin exchange with optically pumped Rb. The apparatus used for ^{3}He, which is described in detail elsewhere (*6, 16*), yielded typically 600–700 cm^3 of gas (standard temperature and pressure, STP) polarized to ≈10% within 8 h.

For ^{129}Xe, a prototype device (Magnetic Imaging Technologies Inc., Durham, NC) capable of polarizing large quantities

according to (*3*) was used. A gas stream containing 1% Xe (natural isotopic composition with 26.4% ^{129}Xe), 1% N_2, and 98% ^{4}He was passed through a Rb vaporizer and then through the optical pumping chamber, which was maintained at 130–150°C and illuminated with circularly polarized light (795 nm) from a 120-W fiber-coupled diode laser array (Opto Power Corp., Tuscon, AZ). ^{129}Xe retains its polarization during freezing (*20*). Therefore, solid Xe (10–20% ^{129}Xe polarization) was extracted downstream by trapping in a cold finger (77 K) in the field of a permanent magnet (0.2 T). Typical accumulation periods were 20–80 min, yielding an amount of Xe ice equivalent to 200–800 cm^3 gas at STP. The complete accumulation system (including cold finger, permanent magnet, and Dewar) was then disconnected and transported to the MRI scanner (approximately 20 min).

All *in vivo* studies were performed using a custom-built, computerized pressure ventilator (*21*). To supply ^{3}He or ^{129}Xe to the ventilator, the polarized noble gas was transferred to a flexible plastic bag serving as the reservoir *R* (capacity, 1000 cm^3). The bag was enclosed in a rigid, sealed Plexiglas cylinder, which was pressurized to control the delivery of HP gas to the animal through a ventilation valve. ^{3}He was released directly into the bag through an outlet port at the polarizing chamber. For experiments with HP ^{129}Xe, the bag was connected to the cold finger, which was placed into boiling water for rapid thawing of the Xe ice. Naturally abundant Xe contains 21.2% quadrupolar ^{131}Xe, which limits the lifetime of the ^{129}Xe spin polarization in the solid state at low magnetic fields due to cross relaxation (*22*). In the gas phase, a significant contribution to relaxation may result from rapid diffusion in a magnetic field gradient. To maintain high ^{129}Xe polarization, thawing was therefore performed close to the bore (30-cm diameter) of the imaging magnet, in a region with a sufficiently high ($>$0.1 T) and homogeneous fringe field. Best results were obtained when the outlet valve at the cold finger was opened with a delay of 8–10 s after inserting into the hot water, to generate elevated pressure, which was then instantaneously released into the bag. To measure the polarization remaining after thawing (typically 2–7%), a glass vessel (100 cm^3) was connected to the cold finger and filled to $\approx$2 atm with HP gas. The amplitude of the HP ^{129}Xe FID was then compared with the signal measured in the same sample after adding 1 atm of air to achieve full relaxation (overnight at 2 T) to the Boltzmann equilibrium.

To maintain anesthesia and normal gas exchange, alternate breaths of air/isoflurane and HP noble gas were provided by the ventilator, which supported independent control of inspiration, held breath periods, and expiration of the animal via pneumatically controlled dual-stage breathing valves. The ventilator computer further supplied an adjustable trigger to the MRI scanner to initiate imaging at specific phases of the breathing cycle. Imaging was done only during noble gas breaths. Breathing rates were 40–60 breaths per min with tidal volumes of 2 cm^3 for ^{3}He and 3–4 cm^3 for Xe.

Animal Preparations

All animal procedures were approved by the Duke University Institutional Animal Care and Use Committee. Adult guinea pigs (Harlan Sprague–Dawley Inc., Indianapolis, IN), ranging from 250–350 g body weight were anesthetized with methohexital sodium (45 mg/kg, Eli Lilly Co., Indianapolis, IN), and a 3.5-cm-long, 14-gauge intracatheter (Sherwood Medical, Tullamore, Ireland) was inserted by tracheostomy to establish a gas-tight connection to the ventilator. During imaging, animals were anesthetized with isoflurane (2–3%). Continuous monitoring of physiologic functions included electrocardiogram from pediatric electrodes taped to the foot pads, temperature from a rectal thermistor, CO_2 in the expired air with a micro-capnometer, and airway pressure from a solid-state pressure transducer on the breathing valve. A comprehensive description of all animal procedures can be found in (*15, 23, 24*).

NMR Procedures

A 2-T, horizontal-bore imaging magnet (Oxford Instruments, Oxford, UK) with shielded gradients (180 mT/m), controlled by a Signa console (General Electric Medical Systems, Milwaukee, WI) was used for all NMR experiments. All RF coils were custom-built with birdcage design (7-cm diameter). For HP ^{3}He experiments, a dual-frequency coil was used, tuned to 85.5 MHz (^{1}H) and 65.1 MHz (^{3}He). Coronal and axial proton scout images were acquired prior to ^{3}He scans to confirm proper localization of the animal (prone position). For HP ^{129}Xe experiments, scout images were first acquired with a separate proton coil. Anatomical landmarks were then used to align the animal within the ^{129}Xe coil (23.7 MHz). Frequency and flip angle adjustments were performed prior to HP gas imaging with thermally polarized gas phantoms (Boltzmann cells) containing ^{3}He/O_2 or Xe/O_2 mixtures at elevated pressure. Before recording the first image, a few breaths of HP gas were given to adjust for bulk magnetic susceptibility shifts after specimen loading and to adjust the receiver gain.

Coronal images were acquired without slice selection using 800 or 1600 radial trajectories of *k*-space (hard RF pulse of 132 μs duration, TR = 5 ms) with effective "echo times" of 260–300 μs to minimize consequences of diffusion. Randomization of the radial angle of the views was performed to suppress artifacts from view variation and motion effects. Images were acquired in synchrony with the HP gas infusion. Varying the trigger delay and the acquisition window permitted the selection of any desired portion of the respiratory cycle.

Summing the magnitude of the first few data points of each view provided an average measure of the temporal changes in the signal from the whole lung. For the ^{3}He images, 75 views were acquired during inspiration (duration 400 ms, trigger delay 25 ms from the beginning of inspiration) and another 25 views immediately following inspiration during held breath. Both periods of the breathing cycle were then analyzed separately with a consistent set of parameters. Additionally, two

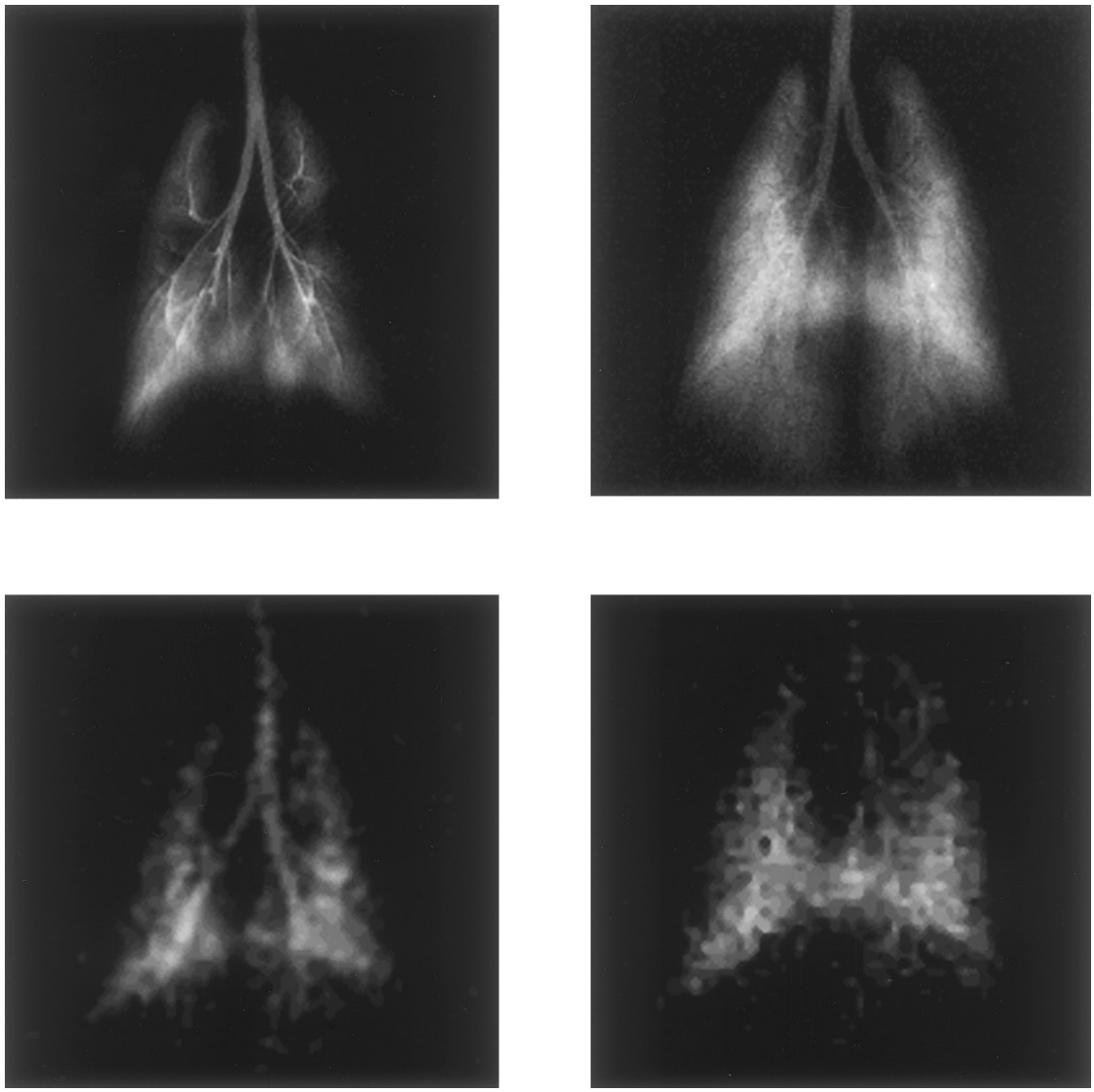

FIG. 2. Non-slice-selective coronal lung images obtained with RA in the living guinea pig in synchrony with HP gas infusion. ^{3}He images (α_B 30°, *TR* 5 ms, 800 views regridded on a 256^2 cartesian matrix, in-plane resolution 188 μm × 188 μm) were recorded during inspiration (top left, acquisition window 100 ms, trigger delay 100 ms from beginning of inspiration) and during held breath (top right, acquisition window 400 ms, trigger delay 50 ms from beginning of held breath). ^{129}Xe images (α_B 20°, *TR* 5 ms, 1600 views regridded on a 128^2 cartesian matrix, resolution 847 μm × 847 μm, acquisition window 400 ms) were recorded during inspiration (bottom left, trigger delay 100 ms from beginning of inspiration) and during held breath (bottom right, trigger delay 50 ms from beginning of held breath).

series of ^{129}Xe images (80 views per breath) measured in different animals during inspiration (duration 500 ms, trigger delay 100 ms from the beginning of inspiration) and held breath (duration 450 ms, trigger delay 50 ms from the beginning of held breath) were included in the quantitative analysis. Flip angles were varied between 10° and 80° for ^{3}He, between 10° and 63° for the ^{129}Xe inspiration study, and between 10° and 32° for the ^{129}Xe held-breath study.

To measure $T'_{1,p}$, the animal received alternate air/isoflurane and HP noble gas breaths for 24 s to build up a steady concentration of HP gas in the lungs. A series of non-localized FIDs (16–64) was then collected during a 24-s suspension of breathing at full inspiration of noble gas. After a 60-s recovery period of air/isoflurane breaths to allow normalization of exhaled CO_2, the complete procedure was repeated with different settings for α (5° and 10°) and *TR* (0.375 and 1.5 s).

RESULTS AND DISCUSSION

Typical HP noble gas lung images acquired *in vivo* in the guinea pig are shown in Fig. 2. Airways appear bright on the images obtained during inspiration because of the continual replenishment of magnetic moment during the acquisition. Although the noble gas fills the entire lung, magnetic moment is destroyed due to RF pulsing before it enters the alveolar space, which therefore is characterized by lower signal inten-

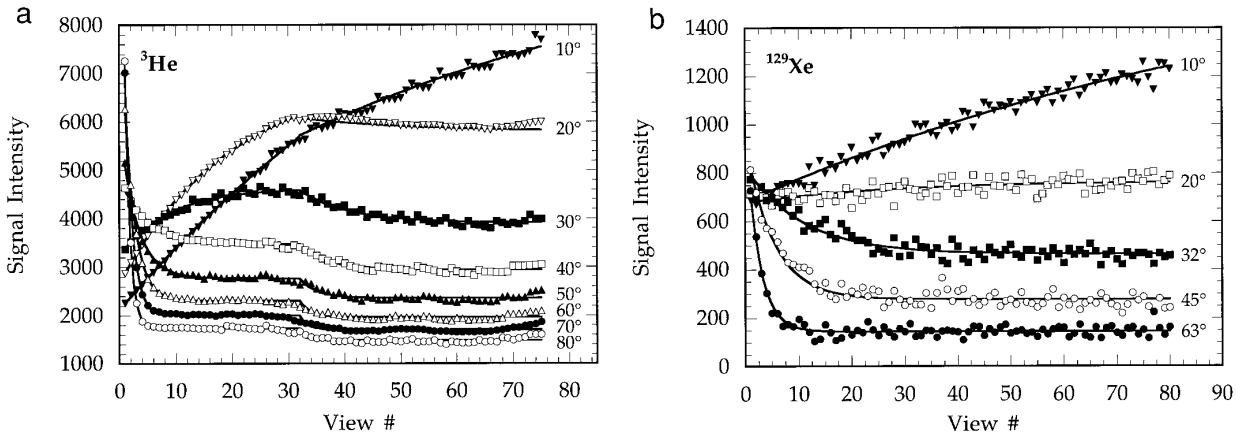

FIG. 3. Signal curves obtained with RA during inspiration (4th noble gas breath) of (a) ^{3}He and (b) ^{129}Xe with different flip angles (^{3}He, α_B 10–80°, *TR* 5 ms, acquisition window 375 ms, trigger delay 25 ms from the beginning of inspiration; ^{129}Xe, α_B 10–63°, *TR* 5 ms, acquisition window 400 ms, trigger delay 100 ms from the beginning of inspiration). Solid lines are results from least-squares fitting to Eq. [17].

sity. This situation may be compared to time-of-flight MR angiography. When imaging at held breath, airway structure is partly obscured on the non-slice-selective images, as now highly polarized gas has also reached the most peripheral airspaces by the beginning of RF application. An examination of the image contrast as a function of various experimental parameters is given elsewhere (*16*). Compared with the ^{3}He results, the ^{129}Xe images show similar characteristics, however, with a significantly decreased signal/noise-ratio (SNR), predominantly due to the combined effects of a lower spin polarization (factor of 2), the lower abundance of the NMR nucleus in the gas mixture (factor of 3.8), and the smaller gyromagnetic ratio (factor of 2.8).

Imaging During Inspiration of HP Noble Gas

Graphical presentations of signal curves obtained with RA MRI during the 4th noble gas inhalation are given in Fig. 3. Due to the delay between the beginning of gas infusion and the start of the scan, the first view already possesses a strong signal, the magnitude of which decreases with sin α as predicted by Eq. [12].

Based on literature data on noble gas relaxation in the presence of molecular oxygen (*25, 26*), we expect both ^{3}He and ^{129}Xe T_1 to be on the order of tens of seconds in the lungs and even longer in the reservoir. With $TR = 5$ ms, the approximations $E_{1,p} \approx 1$ and $E_{1,R} \approx 1$ were justified, and least-squares fitting of the signal curves was performed with the simplified equation (from Eq. [12])

$$S_I(n_j) \propto M_{z,p}(0_j^I)\cos^{n-1}\alpha \sin\alpha + M_{z,I}(0_j)\frac{1-\cos^n\alpha}{1-\cos\alpha}\sin\alpha. \quad [17]$$

Further verification of these assumptions is given below. Results are summarized in Tables 1 and 2 and in Fig. 3. Note that the experimental data were determined as absolute values. An additional fixed parameter according to the observed noise level (18 for ^{3}He and 83 for ^{129}Xe) was therefore considered in the fitting procedures. The experimentally obtained flip angles in the pulmonary gas space, α_p, differed from the adjustments made with Boltzmann cells, α_B, by about 11–16% as a result

TABLE 1
Results Obtained from the Fitting Procedures for the ^{3}He Data[a]

α_B	α_p	$M_{z,p}(0_j^I)$	$M_{z,I}(0_j)$	$M'_{z,I}(0_j)$	n_∞	$S_I(\infty_j)$	$M_{z,diff}(0_j)$
10°	9.0°	13480 ± 110	1026 ± 6	795 ± 5	373	10101 ± 71	521 ± 6
20°	17.9°	8285 ± 43	1105 ± 3	920 ± 2	94	5842 ± 23	645 ± 7
30°	26.9°	6360 ± 64	1103 ± 4	933 ± 3	42	3901 ± 18	669 ± 7
40°	35.8°	6733 ± 38	1118 ± 3	949 ± 4	23	2938 ± 16	821 ± 9
50°	44.8°	6099 ± 50	1139 ± 4	970 ± 5	15	2353 ± 15	810 ± 9
60°	53.7°	6630 ± 40	1167 ± 4	995 ± 5	10	1966 ± 13	881 ± 9
70°	62.7°	6661 ± 42	1218 ± 5	1041 ± 6	7	1709 ± 12	824 ± 9
80°	71.6°	6409 ± 38	1251 ± 6	1069 ± 6	5	1482 ± 11	892 ± 9

[a] Numerical data given for $M_{z,p}(0_j^I)$, $M_{z,I}(0_j)$, $M'_{z,I}(0_j)$, $S_I(\infty_j)$, and $M_{z,diff}(0_j)$ are in arbitrary units and were obtained for the 4th noble gas breath (i.e., $j = 4$).

TABLE 2
Results Obtained from the Fitting Procedures for the ^{129}Xe Data[a]

α_B	α_p	$M_{z,p}(0_j^I)$	$M_{z,I}(0_j)$	n_∞	$S_I(\infty_j)$	$M_{z,p}(0_j^{HB})$
10°	8°	4434 ± 50	113.6 ± 1.0	472	1694 ± 61	3117 ± 33
20°	17°	2172 ± 33	91.8 ± 0.7	105	681 ± 25	1372 ± 25
32°	27°	1647 ± 28	81.8 ± 0.8	41	376 ± 14	624 ± 17
45°	38°	1261 ± 30	59.8 ± 1.1	21	192 ± 8	—
63°	53°	823 ± 21	27.6 ± 1.8	11	62 ± 5	—

[a] Numerical data given for $M_{z,p}(0_j^I)$, $M_{z,I}(0_j)$, $M_{z,p}(0_j^{HB})$, and $S_I(\infty_j)$ are in arbitrary units and were obtained for the 4th noble gas breath (i.e., $j = 4$).

of the difference in loading (^{3}He, $\alpha_p/\alpha_B = 0.8953 \pm 0.0028$; ^{129}Xe, $\alpha_p/\alpha_B = 0.84 \pm 0.11$).

With continuing inspiration of noble gas, the signal curves approach a steady-state, at which the magnetic moment delivered during one *TR* period equals the magnetic moment being destroyed (predominantly by RF) within the same interval. Both the number of views required to reach the steady-state and the respective signal amplitude are functions of the flip angle. For $n \to \infty$, we obtain with Eq. [17] for the steady-state signal amplitude,

$$S_I(\infty_j) \propto M_{z,I}(0_j)\,\frac{\sin\alpha_p}{1-\cos\alpha_p}, \qquad [18]$$

which agrees well with the experimental observations (Fig. 3 and Tables 1 and 2). If we define the steady-state by the condition that all terms of Eq. [17] depending on n have decreased to less than 1% of their initial value, the threshold view number is

$$n_\infty = 1 - \frac{2}{\log(\cos\alpha_p)}. \qquad [19]$$

Numerical results are included in Tables 1 and 2. Consistent with these predictions, a steady-state region was not obtained experimentally for $\alpha_p < 20°$ (Fig. 3). If, however, moderate flip angles were used to capture the signal while the gas was travelling through the conducting airways, the problem of view-to-view variations was inherently minimized by the acquisition scheme without the need of variable flip angle procedures, as suggested by others (*27*).

The pressure curves measured at the transducer typically showed deviations from a linear increase at the beginning of inspiration. For the ^{3}He experiments, fits were therefore performed with two different input terms $M_{z,I}(0_j)$ for the initial 32 views and $M'_{z,I}(0_j)$ for the final period of inhalation. Consequently, the signal curves approached a second plateau level in response to the change in the input function after 32 views (Fig. 3a). This was not observed with ^{129}Xe (Fig. 3b) because a longer trigger delay from the beginning of inspiration (100 ms instead of 25 ms) was used in these studies.

Generally, $M_{z,p}(0_j^I)$ is a metric of how efficiently the polarization is used for the imaging process and should approach zero if no residual magnetic moment is left from previous breaths. However, for the experiments shown in Fig. 3, an additional contribution to $M_{z,p}(0_j^I)$ results from the amount of HP gas delivered during the delay between the beginning of gas infusion and the start of data acquisition. With $TR = 5$ ms, we therefore expect ratios $M_{z,p}(0_j^I)/M_{z,I}(0_j) \approx 5$ for ^{3}He (25 ms trigger delay) and 20 for ^{129}Xe (100 ms trigger delay) in the ideal case. This was observed for ^{3}He and $\alpha_p > 20°$, demonstrating the high precision of the experimental setup (Table 1). For smaller flip angles, residual bulk magnetic moment contributed significantly to $M_{z,p}(0_j^I)$. Note, that the acquisition window included 125 ms of held breath in the ^{3}He studies leading to a quantitative decay of the hyperpolarization for $\alpha_p > 20°$ (Fig. 4). For the ^{129}Xe studies, data acquisition was restricted to inspiration periods, hence increasing contributions to $M_{z,p}(0_j^I)$ from residual magnetic moment were observed when decreasing α_p (Table 2).

Imaging During Held Breath

Using the approximation $E_{1,p} \approx 1$, we expect a signal decay

$$S_{HB}(n_j) \propto M_{z,p}(0_j^{HB})\cos^{n-1}\alpha \sin\alpha \qquad [20]$$

for held breath periods. *In vivo* data and results from least-squares fitting are presented in Fig. 4 and Table 2. Note that $M_{z,p}(0_j^{HB})$ was not a fitting parameter for the ^{3}He curves because held breath and inspiration results were obtained in a single acquisition window; hence $M_{z,p}(0_j^{HB})$ is completely determined by the inspiration results. For ^{129}Xe, the calculated curves agreed well with the observed decays. Deviations from the predictions based upon Eq. [20] resulted, however, for ^{3}He, where less rapid decays were measured. The quality of these fits did not improve when we considered an additional constant input term, which might occur if the inspiration valve did not shut off the noble gas flow completely.

Further data analysis included the effects of gaseous diffusion. The upper parts of the trachea and the endotracheal tube extended outside the birdcage coil. In this region, the RF field intensity is greatly reduced, and even high flip angles do not significantly destroy polarization. For simplicity, we may assume a constant magnetic moment outside the field-of-view (FOV). If diffusion is fast, highly polarized spins are trans-

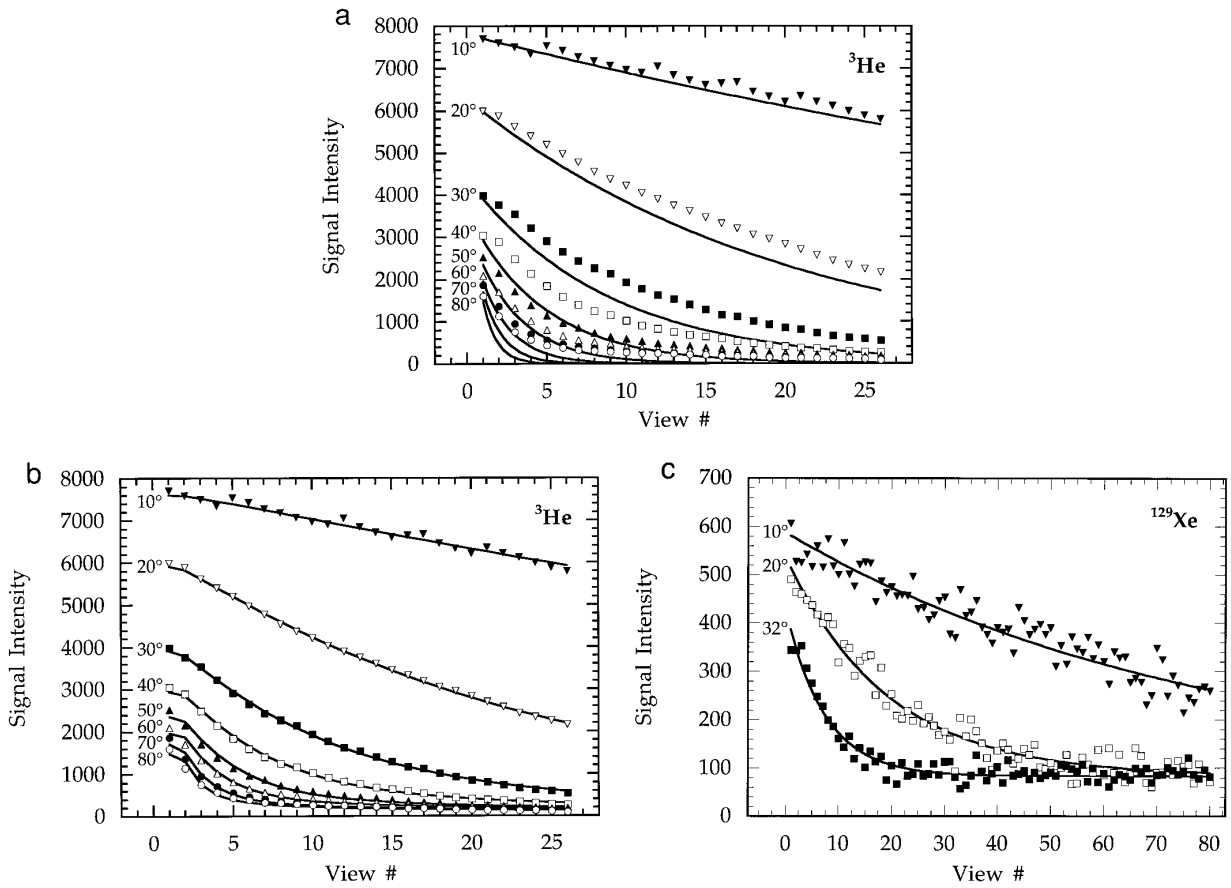

FIG. 4. Signal curves obtained with RA during held breath after inhalation (4th noble gas breath). (a) ^{3}He data (α_B 10–80°, *TR* 5 ms, acquisition window 125 ms at the beginning of held breath) fitted to Eq. [20]; (b) same data fitted to Eq. [21] with consideration of effects from gaseous diffusion; (c) ^{129}Xe data (α_B 10–32°, *TR* 5 ms, acquisition window 400 ms, trigger delay 50 ms from the beginning of held breath) fitted to Eq. [20].

ported efficiently into the sensitive region of the coil. If we approximate the conducting airways as one long cylindrical pipe of constant diameter, straightforward integration of the diffusion equation (*28*) yields the number of polarized spins entering the FOV between successive pulses, $N_{diff} = 2(N_R/V_R)A\sqrt{DTR/\pi}$, where A is the cross-sectional area of the trachea and D is the diffusion coefficient. The magnetic moment immediately before the nth RF pulse of the jth held breath period thus has to be corrected by an additional term, according to

$$M_{z,p}(n_j^-) = M_{z,p}(n - 1_j^-)\cos\alpha + M_{z,diff}(0_j)[\sqrt{n - 1_j} - \sqrt{n - 2_j}], \quad [21]$$

with

$$M_{z,diff}(0_j) = 2M_{z,R}(0_j)\frac{A}{V_R(0)}\sqrt{\frac{DTR}{\pi}}. \quad [22]$$

Signal decays obtained with Eq. [21] agreed well with the experimental data as shown in Fig. 4b. Numerical results are included in Table 1.

The results for $M_{z,diff}$ and $M_{z,I}$ were used to estimate the diffusion coefficient with the aid of Eqs. [5] and [22] according to

$$D = \left[\frac{M_{z,diff}(0_j)}{M_{z,I}(0_j)}\frac{V_T}{2A\tau_I}\right]^2 \pi TR. \quad [23]$$

Assuming $A = 0.07$ cm^2 for the guinea pig trachea, we obtain $D = 8.9 \pm 2.3$ cm^2/s with the data in Table 1 and the acquisition parameters ($V_T = 2$ cm^3, $\tau_I = 400$ ms, $TR = 5$ ms). This value is much larger than an estimate of the ^{3}He self diffusion coefficient of 1.96 cm^2/s at 1 atm and 37°C based on literature data (*29*). The discrepancy is most likely explained by an additional contribution from convection of ^{3}He in the airways. Note that data acquisition for the ^{3}He held breath studies started immediately after inspiration, leading to experimental conditions, for which considerable overestimations of D have to be expected (*28*). For Xe, the self diffusion coefficient is only 0.06 cm^2/s (*29*), hence we may not expect a

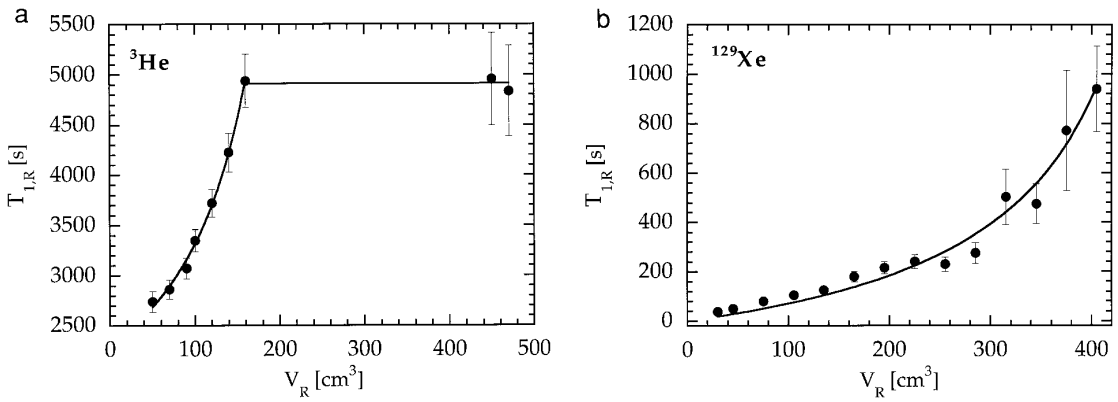

FIG. 5. Variation of the spin–lattice relaxation time in the noble gas reservoir, $T_{1,R}$, with the reservoir volume, V_R, for (a) ^{3}He and (b) ^{129}Xe. The solid lines serve as guides to the eye.

significant contribution from $M_{z,diff}$ in the ^{129}Xe results. In addition, convection effects were reduced due to the trigger delay between the end of inspiration and start of data acquisition in the ^{129}Xe held breath study. Consequently, good fits were obtained with the simple Eq. [20] in these cases.

Spin–Lattice Relaxation

Beginning with 80°, α_B was reduced in increments of 10° for the ^{3}He studies, whereas both series of ^{129}Xe experiments started with the smallest flip angle. Inspection of the results in Tables 1 and 2 indicates parallel decays for $M_{z,I}$, $M'_{z,I}$, and $M_{z,diff}$ during the course of the experiments. This observation can be explained by spin–lattice relaxation in the HP gas reservoir as predicted by Eq. [5].

Additional results were obtained when larger data sets from three-dimensional imaging experiments were analyzed. As a general finding, both ^{3}He and ^{129}Xe showed significant deviations from exponential decays of $M_{z,I}$ during longer imaging periods. In the absence of impurities (especially molecular oxygen), $T_{1,R}$ is dominated by interactions with the container surface. Due to the flexibility of the polyethylene bag that was used, its surface area stayed constant throughout the experiment, while V_R was reduced by V_T with each noble gas breath. Consequently, the surface relaxation gained importance parallel to the reservoir volume reduction during the course of the experiment, hence leading to a change in $T_{1,R}$. Figure 5 shows results obtained from separate analyses of sections of the $M_{z,I}$ decays with sufficiently small variations in V_R. For ^{3}He, $T_{1,R}$ was constant (4911 ± 66 s) if the bag was filled to >160 cm^3 but decreased to 2740 ± 110 s at $V_R \approx 50$ cm^3. For ^{129}Xe, a continous decay of $T_{1,R}$ from 940 ± 180 s ($V_R \approx 405$ cm^3) to 38.9 ± 6.3 s ($V_R \approx 30$ cm^3) was found (data referring to room temperature and ≈0.1 T, i.e., the fringe field at the position of the reservoir). Consistent with expectations, our observations indicate a significantly shorter surface residence time for ^{3}He, hence minor importance of surface relaxation, as compared with ^{129}Xe.

With typical durations of HP gas imaging experiments below a minute, the ^{3}He signal loss due to relaxation in the reservoir will be on the order of 2% and still less than 50% for long studies up to 30 min. In contrast, the measured $T_{1,R}$ data indicate a relevant decay of polarization during the course of ^{129}Xe studies due to the increasing importance of surface relaxation effects. Better results were obtained recently when using a Tedlar bag (Jensen Inert, Coral Springs, FL) instead of polyethylene, yielding ^{129}Xe $T_{1,R}$ values similar to the ^{3}He data shown in Fig. 5a. Careful choice of materials thus helps support longer acquisition periods, which may be of particular importance for MR microscopy in small animals.

The acquisition windows used for our imaging experiments (≤500 ms) are not sensitive to effects from spin–lattice relaxation if $T'_{1,p}$ is well above 1 s. For reliable estimates, the held breath period was therefore extended to 24 s by suspending breathing, as described under Methods, while signal decay curves were recorded with non-selective RF pulse trains. While the relaxation-related signal loss only depends on the total observation time, the parallel loss due to RF pulsing can easily be eliminated by varying the flip angle or repetition time in a series of experiments. Results obtained with least-squares fitting (four data sets for each nucleus) were $T'_{1,p} = 28.8 \pm 1.8$ s for ^{3}He and $T'_{1,p} = 31.3 \pm 1.8$ s for ^{129}Xe. The ^{3}He data agree well with previous measurements in the human lung, where $T'_{1,p} = 36$ s was reported (*10*).

If we assume that noble gas relaxation in the lungs is entirely dominated by intermolecular magnetic dipole coupling with molecular oxygen, we may calculate the alveolar partial pressure of O_2 (P_{AO_2}) using literature results on ^{3}He and ^{129}Xe relaxation in the presence of O_2 (*25, 26*). Using the above values for $T'_{1,p}$, we obtained $P_{AO_2} = 78$ mmHg from the ^{3}He data and $P_{AO_2} = 83$ mmHg from the ^{129}Xe data. This compares well with rough estimates of 76–93 mmHg for the situation after 24 alternate breaths of air and noble gas. To estimate P_{AO_2} in the guinea pig lung, we used tidal volumes of 2 cm^3 ^{3}He, 3 cm^3 Xe, and 4.2 cm^3 air, a functional residual capacity of 8 cm^3 and treated ventilation as a discontinuous process (*19*). Regarding the excellent agreement of these results, we conclude that

the assumption of a dominant contribution from relaxation via paramagnetic O_2 in the lung is valid. It further indicates that the polarization losses due to gas uptake by the pulmonary blood are negligible for both ^{3}He and ^{129}Xe compared with spin–lattice relaxation (i.e., $T'_{1,p} \approx T_{1,p}$).

With the results for $T_{1,R}$ and $T'_{1,p}$, we find all terms $E_{1,R}^{n-1}$, $E_{1,p}^{n-1}$, and $(E_{1,p}/E_{1,R})^n$ being greater than 0.98 for our imaging studies, providing experimental verification of the approximations used above to derive Eqs. [17] and [20]. It also underlines that spin–lattice relaxation effects do not preclude biomedical MRI with HP gases.

CONCLUSIONS

An analytical model describing signal dynamics in lung MRI with HP noble gases that includes explicit consideration of the breathing cycle has been constructed. Agreement between theoretical predictions and *in vivo* results is excellent for studies with ^{3}He as well as with ^{129}Xe. The model may be used to select an optimum flip angle or to address consequences of view variations for a given sampling strategy through any part of the breathing cycle. Additionally, extensive information about noble gas relaxation in the pulmonary gas space and in the holding reservoir was obtained. Besides the fundamental importance for lung imaging, such data are crucial for feasibility calculations of future experiments (e.g., perfusion studies) involving HP gas delivery via the respiratory system. Regarding recent success in human studies, there is little doubt that HP gas MRI will become a relevant clinical tool in pulmonary medicine. Understanding the polarization dynamics quantitatively will help us to optimize sequence design and to exploit the whole range of applications of this new technology effectively.

ACKNOWLEDGMENTS

This work was supported by grants from the National Center for Research Resources (P41 RR 05959) and the National Science Foundation (CDR-8622201). H.E.M. acknowledges a research fellowship from the Deutsche Forschungsgemeinschaft (Mo 588/3-1), and M.S.C. acknowledges a fellowship from the Whitaker Foundation. The authors thank Gary P. Cofer, Steve A. Suddarth, and John P. O'Donnell for technical support, C. Ted Wheeler for animal preparation, and Elaine G. Fitzsimons for editorial assistance.

REFERENCES

1. W. Happer, E. Miron, S. Schaefer, D. Schreiber, W. A. van Wijngaarden, and X. Zeng, Polarization of the nuclear spin of noble-gas atoms by spin exchange with optically pumped alkali-metal atoms, *Phys. Rev. A* **29,** 3092–3110 (1984).
2. T. Chupp, M. Wagshul, K. Coulter, A. McDonald, and W. Happer, Polarized high-density gaseous ^{3}He targets, *Phys. Rev. C* **36,** 2244–2251 (1987).
3. B. Driehuys, G. D. Cates, E. Miron, K. Sauer, D. K. Walter, and W. Happer, High-volume production of laser-polarized ^{129}Xe, *Appl. Phys. Lett.* **69,** 1668–1670 (1996).
4. G. Eckert, W. Heil, M. Meyerhoff, E. W. Otten, R. Surkau, M. Werner, M. Leduc, P. J. Nacher, and L. D. Schearer, A dense polarized ^{3}He target based on compression of optically pumped gas, *Nucl. Instrum. Meth. A* **320,** 53–65 (1992).
5. M. S. Albert, G. D. Cates, B. Driehuys, W. Happer, B. Saam, C. S. Springer, Jr., and A. Wishnia, Biological magnetic resonance imaging using laser-polarized ^{129}Xe, *Nature* **370,** 199–201 (1994).
6. H. Middleton, R. D. Black, B. Saam, G. D. Cates, G. P. Cofer, R. Guenther, W. Happer, L. W. Hedlund, G. A. Johnson, K. Juvan, and J. Swartz, MR imaging with hyperpolarized ^{3}He gas, *Magn. Reson. Med.* **33,** 271–275 (1995).
7. R. D. Black, H. L. Middleton, G. D. Cates, G. P. Cofer, B. Driehuys, W. Happer, L. W. Hedlund, G. A. Johnson, M. D. Shattuck, and J. C. Swartz, In vivo He-3 MR images of guinea pig lungs, *Radiology* **199,** 867–870 (1996).
8. M. E. Wagshul, T. M. Button, H. F. Li, Z. Liang, C. S. Springer, K. Zhong, and A. Wishnia, In vivo MR imaging and spectroscopy using hyperpolarized ^{129}Xe, *Magn. Reson. Med.* **36,** 183–191 (1996).
9. K. Sakai, A. M. Bilek, E. Oteiza, R. L. Walsworth, D. Balamore, F. A. Jolesz, and M. S. Albert, Temporal dynamics of hyperpolarized ^{129}Xe resonances in living rats, *J. Magn. Reson. B* **111,** 300–304 (1996).
10. P. Bachert, L. R. Schad, M. Bock, M. V. Knopp, M. Ebert, T. Großmann, W. Heil, D. Hofmann, R. Surkau, and E. W. Otten, Nuclear magnetic resonance imaging of airways in humans with use of hyperpolarized ^{3}He, *Magn. Reson. Med.* **36,** 192–196 (1996).
11. J. R. MacFall, H. C. Charles, R. D. Black, H. Middleton, J. C. Swartz, B. Saam, B. Driehuys, C. Erickson, W. Happer, G. D. Cates, G. A. Johnson, and C. E. Ravin, Human lung air spaces: Potential for MR imaging with hyperpolarized He-3, *Radiology* **200,** 553–558 (1996).
12. H. U. Kauczor, D. Hofmann, K. F. Kreitner, H. Nilgens, R. Surkau, W. Heil, A. Potthast, M. V. Knopp, E. W. Otten, and M. Thelen, Normal and abnormal pulmonary ventilation: Visualization at hyperpolarized He-3 MR imaging, *Radiology* **201,** 564–568 (1996).
13. H. U. Kauczor, M. Ebert, K. F. Kreitner, H. Nilgens, R. Surkau, W. Heil, D. Hofmann, E. W. Otten, and M. Thelen, Imaging of the lungs using 3He MRI: Preliminary clinical experience in 18 patients with and without lung disease, *J. Magn. Reson. Imag.* **7,** 538–543 (1997).
14. J. P. Mugler III, B. Driehuys, J. R. Brookeman, G. D. Cates, S. S. Berr, R. G. Bryant, T. M. Daniel, E. E. de Lange, J. H. Downs III, C. J. Erickson, W. Happer, D. P. Hinton, N. F. Kassel, T. Maier, C. D. Phillips, B. T. Saam, K. L. Sauer, and M. E. Wagshul, MR imaging and spectroscopy using hyperpolarized ^{129}Xe gas: Preliminary human results, *Magn. Reson. Med.* **37,** 809–815 (1997).
15. G. A. Johnson, G. Cates, X. J. Chen, G. P. Cofer, B. Driehuys, W. Happer, L. W. Hedlund, B. Saam, M. D. Shattuck, and J. Swartz, Dynamics of magnetization in hyperpolarized gas MRI of the lung, *Magn. Reson. Med.* **38,** 66–71 (1997).
16. X. J. Chen, M. S. Chawla, L. W. Hedlund, H. E. Möller, J. R. MacFall, and G. A. Johnson, MR microscopy of lung airways with hyperpolarized ^{3}He, *Magn. Reson. Med.* **39,** 79–84 (1998).
17. J. H. Gao, L. Lemen, J. Xiong, B. Patyal, and P. T. Fox, Magnetization and diffusion effects in NMR imaging of hyperpolarized substances, *Magn. Reson. Med.* **37,** 153–158 (1997).
18. M. D. Shattuck, S. L. Gewalt, G. H. Glover, L. W. Hedlund, and G. A. Johnson, MR microscopy of the lung using volume projection encoding, *Magn. Reson. Med.* **38,** 938–942 (1997).
19. S. S. Kety, The theory and applications of the exchange of inert gas at the lungs and tissues, *Pharmacol. Rev.* **3,** 1–41 (1951).
20. G. D. Cates, D. R. Benton, M. Gatzke, W. Happer, K. C. Hasson, and N. R. Newbury, Laser production of large nuclear-spin polarization in frozen xenon, *Phys. Rev. Lett.* **65,** 2591–2594 (1990).

21. L. W. Hedlund, M. D. Shattuck, and G. A. Johnson, Three-dimensional MR microscopy of pulmonary dynamics, *in* "Proceedings of the International Society for Magnetic Resonance in Medicine, 4th Scientific Meeting, New York, 1996," p. 327.

22. M. Gatzke, G. D. Cates, B. Driehuys, D. Fox, W. Happer, and B. Saam, Extraordinary slow nuclear spin relaxation in frozen laser-polarized ^{129}Xe, *Phys. Rev. Lett.* **70,** 690–693 (1993).

23. G. A. Johnson, H. Beneviste, R. D. Black, L. W. Hedlund, R. R. Maronpot, and B. R. Smith, Histology by magnetic resonance microscopy. *Magn. Reson. Quart.* **9,** 1–30 (1993).

24. H. H. Qiu, G. P. Cofer, L. W. Hedlund, and G. A. Johnson, Automated feedback control of body temperature for small animals studies with MR microscopy, *IEEE Trans. Biomed. Eng.* **44,** 1107–1113 (1997).

25. C. J. Jameson, A. K. Jameson, and J. K. Hwang, Nuclear spin relaxation by intermolecular magnetic dipole coupling in the gas phase, ^{129}Xe in oxygen, *J. Chem. Phys.* **89,** 4074–4081 (1988).

26. B. Saam, W. Happer, and H. Middleton, Nuclear relaxation of ^{3}He in the presence of O_2, *Phys. Rev. A* **52,** 862–865 (1995).

27. L. Zhao, R. Mulkern, C. H. Tseng, D. Williamson, S. Patz, R. Kraft, R. L. Walsworth, F. A. Jolesz, and M. S. Albert, Gradient-echo imaging considerations for hyperpolarized ^{129}Xe MR, *J. Magn. Reson. B* **113,** 179–183 (1996).

28. W. Jost, "Diffusion," pp. 30–35, Steinkopff, Darmstadt (1957).

29. Landolt-Börnstein, "Zahlenwerte und Funktionen aus Physik, Chemie, Astronomie, Geophysik und Technik," II. Band, 5. Teil (H. Borchers, H. Hausen, K. H. Hellwege, K. Schäfer, and E. Schmidt, Eds.), 6th ed., pp. 516–523, Springer-Verlag, Berlin (1969).